ELSEVIER

Journal of Alloys and Compounds 216 (1994) 1–6

Journal of ALLOYS AND COMPOUNDS

Hydride formation in two-phase ($Ti_3Al + TiAl$) titanium aluminides during cathodic charging and its dissociation

Akito Takasaki, Kozo Ojima, Youji Taneda

Department of Mathematics and Physics, National Defense Academy, 1-10-20 Hashirimizu, Yokosuka, Kanagawa 239, Japan

Received 13 December 1993

Abstract

A $(TiAl)H_x$ hydride which has a tetragonal crystal structure with lattice parameters $a = 0.452$ nm and $c = 0.326$ nm ($c/a = 0.721$) has been observed in Ti–42Al, Ti–45Al and Ti–50Al (at.%) two-phase (Ti_3Al (α_2) + TiAl (γ)) titanium aluminides by cathodic charging in a 5% H_2SO_4 solution. Cracks or pits are also observed within the γ phase regions in the two-phase ($\alpha_2 + \gamma$) coexisting grains (such as lamellar grains) but not within the α_2 phase or single γ grains. Weights of the samples decrease with increasing charging time owing to the crack or pit formation, and this is more drastic in the Ti–50Al alloy than in the Ti–42Al and Ti–45Al alloys. The hydride is thermally stable at temperatures up to about 550 K (277 °C) and dissociates completely at temperatures between 673 K (400 °C) and 723 K (450 °C).

Keywords: Hydride formation; Titanium aluminides; Cathodic charging

1. Introduction

Intermetallic titanium aluminides have attractive specific properties including strength at elevated temperatures and creep resistance [1]. The focus of effort to develop titanium aluminides for high temperature applications has been improved ductility and toughness at room temperature as well as oxidation property at elevated temperatures [2].

Recently considerable effort has been directed towards determining the hydrogen susceptibility of Ti_3Al (α_2) and TiAl (γ), because these alloys have potential applications in aircraft and spacecraft components. Hydrogen is known to cause embrittlement in many alloys, and several titanium aluminides are also reported to be susceptible to hydrogen embrittlement. For instance, it was recently reported for a Ti–24Al–11Nb (at.%) alloy (α_2-based alloy) that the yield strength increased with increasing amount of hydride but the ultimate tensile strength, ductility and fracture toughness decreased [3].

We have already reported that a hydride phase based on $(TiAl)H_x$, which has a tetragonal crystal structure with lattice parameters $a = 0.452$ nm and $c = 0.326$ nm ($c/a = 0.721$), formed in a Ti–42Al ($\alpha_2 + \gamma$ two-phase) alloy during cathodic charging, and charging-induced damage such as cracking on the sample surface was also observed [4]. However, it was difficult at that time to find a microstructural dependence on the hydride or crack formation. Thus we investigate in this paper the effect of microstructure (α_2 and γ) on the formation of hydride and charging-induced damage. The thermal stability and dissociation process of the hydride are also investigated.

2. Experimental procedure

The materials used for this study were Ti–42Al, Ti–45Al and Ti–50Al (at.%) alloys which were arc melted in an argon gas atmosphere. All ingots were wrapped in tantalum foils and the Ti–42Al alloy was homogenized at 1273 K for 604.8 ks (168 h), the Ti–45Al alloy at 1673 K for 14.4 ks (4 h) and then annealed at 1373 K for 1.8 ks (0.5 h), and the Ti–50Al alloy at 1673 K for 14.4 ks (4 h) in an argon gas atmosphere. All ingots were cooled in a furnace under an argon gas flow after heat treatment. Samples of dimensions $10 \times 10 \times 1$ mm^3 were cut from the ingots, mechanically ground with #1200 emery paper and then polished. Hydrogen charging was performed cathodically at room temperature using platinum counter-electrodes in a 5%

SSDI 0925-8388(94)01238-D

H_2SO_4 solution. The current density was maintained at a constant 5 kA m^{-2} and the charging time was varied from 1.8 ks (0.5 h) to 14.4 ks (4 h) to control the hydrogen content in the samples.

The samples before and after hydrogen charging were examined by a Jeol JDX-3530 X-ray diffractometer with Cu Kα radiation operated at 40 kV and 40 mA. The sample surfaces were also observed by an analytical scanning electron microscope ABT DS-130C operated at 15 kV. Sample weights before and after hydrogen charging were measured by an analytical balance.

3. Results

3.1. Microstructures before hydrogen charging

The X-ray diffraction profiles of the Ti–42Al, Ti–45Al and Ti–50Al alloys before hydrogen charging are shown in Figs. 1(a)–1(c) respectively. These X-ray profiles were obtained under rotation of the samples during X-ray diffraction measurement to eliminate a diffraction effect from preferred orientations of the samples. The $201\alpha_2$ diffraction intensity decreases with increasing aluminium content compared with the $002\alpha_2+111\gamma$ combined diffraction intensities, which indicates that the ratio α_2/γ decreases with increasing aluminium content.

The typical microstructures of the three alloys are shown in Fig. 2. The Ti–42Al and Ti–45Al alloys show a lamellar structure which consists of alternating plates of the α_2 and γ phases, but the mean size of the lamellar grains in the Ti–45Al alloy is much larger than that in the Ti–42Al alloy. The microstructure of the Ti–50Al alloy exhibits some equiaxed γ grains and grains consisting of α_2 laths sandwiched by γ bands. Gao et al. called this kind of microstructure a mixture of lamellar and Widmanstätten structures [5].

3.2. Hydride formation

As mentioned earlier, we have already reported that a $(TiAl)H_x$ hydride with a tetragonal crystal structure formed in the Ti–42Al alloy. X-Ray diffraction results for the Ti–45Al and Ti–50Al alloys as well as the Ti–42Al alloy before and after hydrogen charging are shown in Fig. 3. New diffraction peaks are also observed for the Ti–45Al and Ti–50Al alloys and the values of the diffraction angles (2θ) for these new peaks are exactly the same as those of the Ti–42Al alloy, indicating

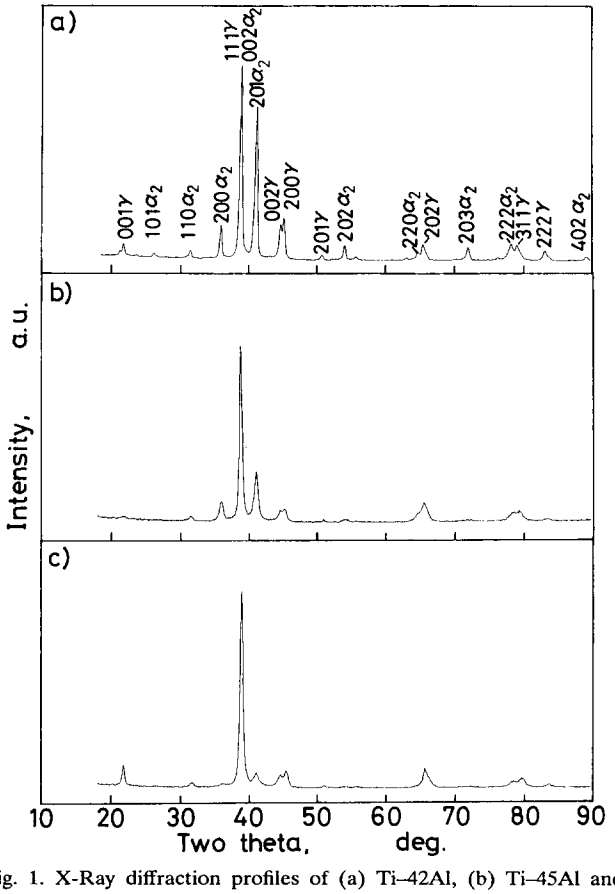

Fig. 1. X-Ray diffraction profiles of (a) Ti–42Al, (b) Ti–45Al and (c) Ti–50Al alloys before hydrogen charging.

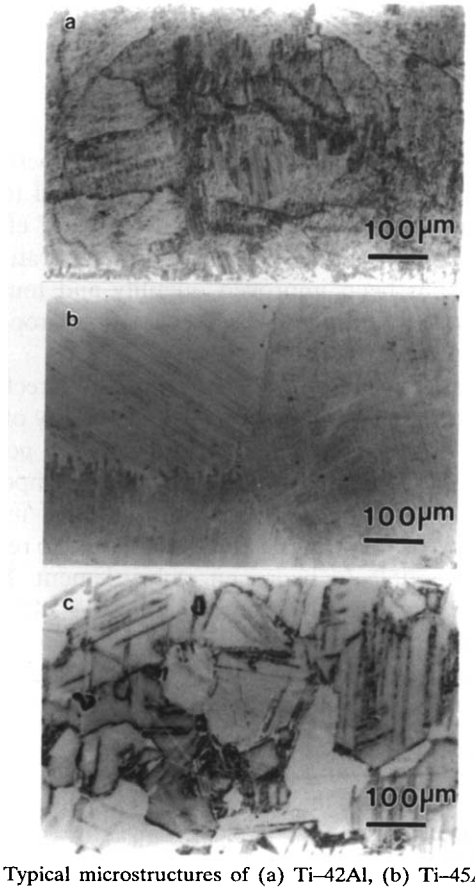

Fig. 2. Typical microstructures of (a) Ti–42Al, (b) Ti–45Al and (c) Ti–50Al alloys before hydrogen charging.

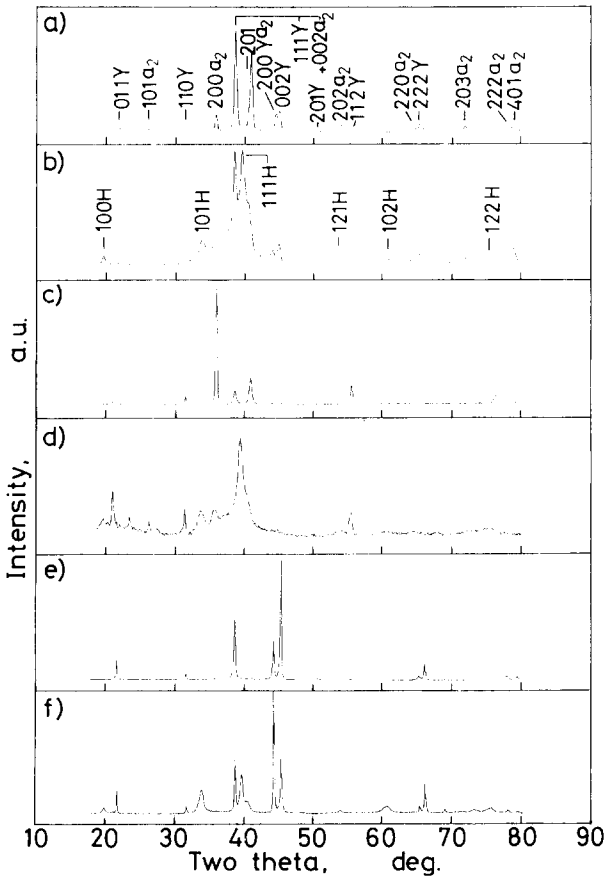

Fig. 3. X-Ray diffraction profiles of Ti–42Al alloy (a) before charging and (b) after charging for 7.2 ks, Ti–45Al alloy (c) before charging and (d) after charging for 7.2 ks, and Ti–50Al alloy (e) before charging and (f) after charging for 7.2 ks.

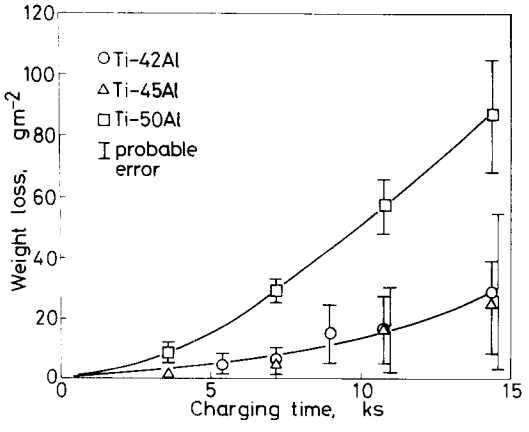

Fig. 4. Sample weight variations during hydrogen charging.

that the same kind of hydride as formed in the Ti–42Al alloy is also observed in the Ti–45Al and Ti–50Al alloys. Details of the X-ray diffraction data for the hydride formed in the Ti–42Al alloy have already been described [4].

The weight variations of the samples during cathodic charging are shown in Fig. 4. The probable errors, which may be due to an inhomogeneous hydrogen distribution on the sample surfaces during cathodic charging, increase with increasing charging time. However, it is suggested that the weight losses of the Ti–42Al and Ti–45Al alloys are almost the same after a given charging time, whereas the weight loss of the Ti–50Al alloy is much larger than those of the Ti–42Al and Ti–45Al alloys. The results of scanning electron microscopy (SEM) observation and energy-dispersive X-ray (EDX) analysis for the Ti–45Al alloy are shown in Fig. 5. Cracks were observed within the lamellae after hydrogen charging for 3.6 ks (Fig. 5(b)) compared with the sample before charging (Fig. 5(a)). On the sample surface after hydrogen charging for 14.4 ks (Fig. 5(c)), the cracks change morphologically into pits, which seem to be geometrically similar to those caused by pitting corrosion, along and within certain lamellae. The EDX results (Fig. 5(d)) indicate that the lamellae with cracks or pits are aluminium rich, whereas the undamaged lamellae are titanium rich. This means that the surface damage (cracks or pits) is observed in the γ phase but not in the α_2 phase. From SEM observation and EDX analysis of the Ti–50Al alloy (Fig. 6), cracks are also observed within two-phase ($\alpha_2+\gamma$) coexisting grains but not within equiaxed single γ grains. Furthermore, the EDX results (Fig. 6(d)) also indicate that the damaged regions are somewhat enriched in aluminium compared with the undamaged regions. This suggests that the surface damage in the Ti–50Al alloy is observed in the γ phase in two-phase coexisting grains but not in the α_2 phase or single γ grains, which agrees fairly well with the results for the Ti–45Al alloy.

3.3. Hydride dissociation

The hydride phase formed in all alloys in this study is similar in crystal form, so the hydride dissociation

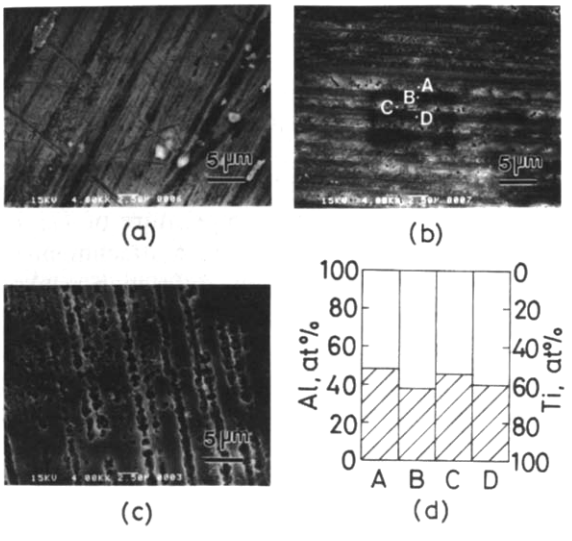

Fig. 5. Surfaces of Ti–45Al alloy (a) before charging, (b) after charging for 3.6 ks and (c) after charging for 14.4 ks, and (d) EDX results for regions marked in (b).

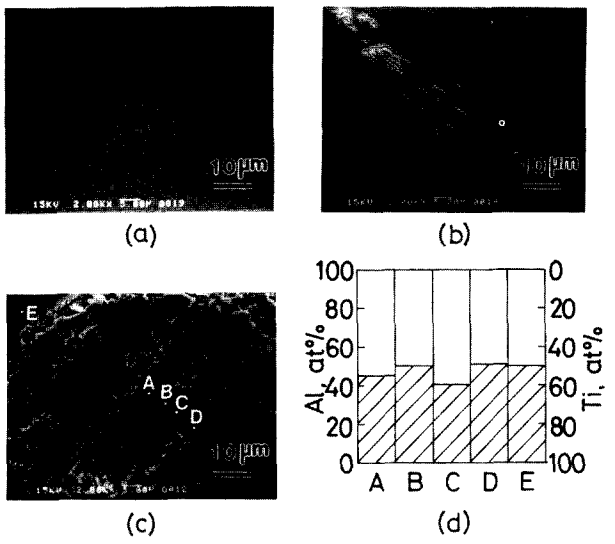

Fig. 6. Surfaces of Ti–50Al alloy (a) before charging, (b) after charging for 3.6 ks and (c) after charging for 14.4 ks, and (d) EDX results for regions marked in (c).

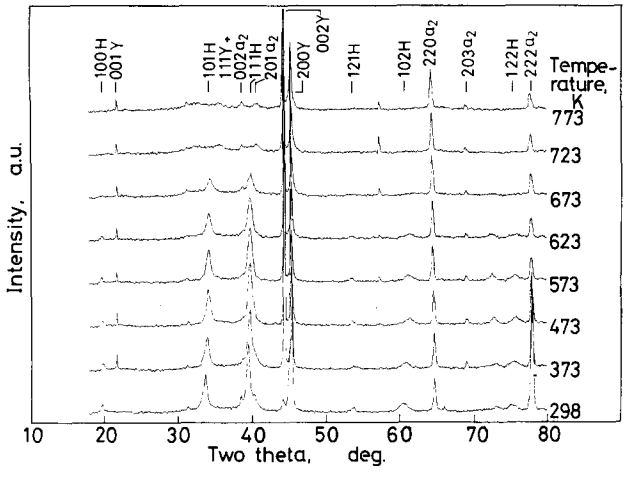

Fig. 7. High temperature X-ray diffraction profiles of Ti–50Al alloy after hydrogen charging for 7.2 ks.

process during heating was examined with the Ti–50Al alloy. The results of in situ high temperature X-ray diffraction measurement for the Ti–50Al alloy after hydrogen charging for 7.2 ks are shown in Fig. 7. Heating of the sample to a temperature of 773 K was performed with a high temperature attachment under an argon gas flow. The X-ray diffraction peaks corresponding to the hydride phase become weaker with increasing heat temperature and disappear at temperatures between 673 and 723 K, when the weak diffraction peaks corresponding to the matrix $(\alpha_2+\gamma)$ reappear. The temperature variations of the two strongest diffraction intensities of the hydride (111 and 101) are shown in Fig. 8. Both integrated intensities almost do not change from room temperature to about 573 K but start to decrease at temperatures above 573 K. This indicates that the hydride phase is thermally stable

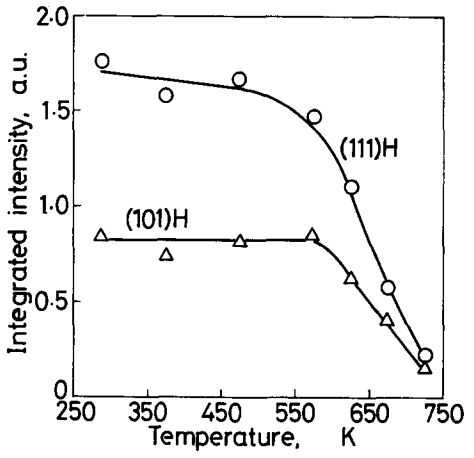

Fig. 8. Temperature variations of X-ray integrated intensities of hydride formed in Ti–50Al alloy.

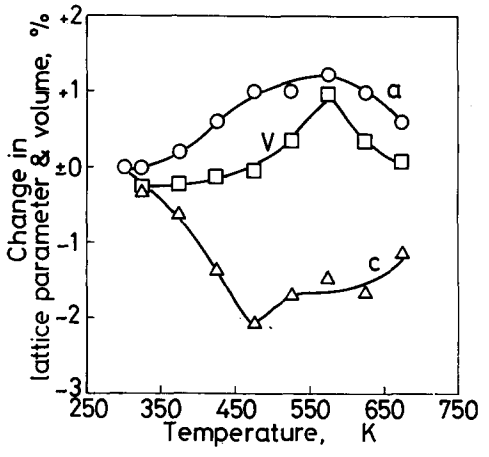

Fig. 9. Changes in lattice parameters and associated crystal volume of hydride during heating.

at heating temperatures up to 573 K but starts to dissociate at temperatures above 573 K and dissociates completely at temperatures between 673 and 723 K. Figure 9 shows the temperature variations of the lattice parameters and the associated lattice volume of the hydride. The *a* axis of the hydride lattice expands at temperatures up to about 573 K while the *c* axis shrinks, and as a result the volume of the hydride lattice increases with increasing temperature up to 573 K.

4. Discussion

Several hydride phases have been reported to form by cathodic charging in titanium aluminides as shown in Table 1, in which our data are also included. It is recognized that most of the hydrides reported are focused on α_2-based alloys and fewer on two-phase $(\alpha_2+\gamma)$ alloys or single γ alloys. The hydride reported in Ref. [11], which formed in a Ti–49.9Al alloy, seems to be the same in crystal structure and chemical form as the hydride observed in this study.

Table 1
Summary of reported hydride phases due to cathodic charging

Hydride	Crystal structure (nm)	Alloy	Charging condition	Remark[a]	Ref.
(TiNb)H		Ti–24Al–11Nb	1 N H_2SO_4 5 kA m^{-2}	HIC	[6]
γ	F.c.t., $a=0.426$, $c=0.475$	Ti–25Al–10Nb–3V–1Mo	1 N H_2SO_4 1 kA m^{-2}	HIC	[7]
δ	F.c.c., $a=0.445$				
$(Ti_3Al)H$	H.c.p., $a=0.587$, $c=0.473$	Ti–24Al–11Nb	1 N H_2SO_4 0.5–1 kA m^{-2}	HIC	[8]
δ	F.c.c., $a=0.445$	Ti–24Al–11Nb	1 N H_2SO_4 2 kA m^{-2}		[9]
		Ti–24Al–11Nb	0.5 N H_2SO_4		[10]
(TiAl)H	Tetragonal, $a=0.452$, $c=0.326$	Ti–42Al	5% H_2SO_4 5 kA m^{-2}	HIC	[4], this study
(TiAl)H	Tetragonal, $a=0.452$, $c=0.326$	Ti–45Al	5% H_2SO_4 5 kA m^{-2}	HIC	This study
(TiAl)H	Tetragonal, $a=0.450$, $c=0.327$	Ti–49.9Al	1 mol l^{-1} NaOH 0.3 kA m^{-2}	Single γ and $\gamma+\alpha_2$	[11]
(TiAl)H	Tetragonal, $a=0.452$, $c=0.327$	Ti–50Al	5% H_2SO_4 5 kA m^{-2}	HIC $\gamma+\alpha_2$	This study
$(Ti_3Al)H$	H.c.p., $a=0.518$, $c=0.518$	Ti–50Al	pH 0.3, 0.6 N H_2SO_4 1 kA m^{-2}		[12]

[a]HIC, hydrogen-induced cracking.

It is widely considered that the α_2 phase takes up hydrogen much more readily than the γ phase [13], and because of the low terminal solubility of hydrogen in the α_2 alloys, almost all hydrogen in a precharged α_2 phase exists as a hydride, whereas the γ alloys almost do not take up hydrogen because of lower hydrogen solubility than the α_2 alloys [14]. We suggest that these considerations are related to gaseous hydrogen phenomena, which could be different from phenomena due to cathodic charging. Our present data on weight variations of samples during cathodic charging (Fig. 4) and our EDX results (Figs. 5 and 6) suggest that possible cracking sites are within the γ phase in two-phase ($\alpha_2+\gamma$) coexisting grains, but no damage is observed in the α_2 phase or equiaxed single γ grains. This indicates that the γ phase in lamellar grains is much more sensitive to cathodic charging than the α_2 phase or equiaxed single γ grains. We also consider that a hydride with the chemical formula $(TiAl)H_x$ would form in/on the γ phase, because diffusions of aluminium and titanium are limited at room temperature. These results obtained by us by cathodic charging seem to be different from those obtained by gaseous hydrogen charging.

From our results, three models for crack or pit formation during cathodic charging could be considered and these are shown schematically in Fig. 10. The first model (Fig. 10(a)) follows the gaseous hydrogen phenomena which were mentioned above. The α_2 phase takes up much more hydrogen than the γ phase, so that the α_2 phase easily expands much more than the γ phase. As a result, the γ phase, whose yield strength is generally less than that of the α_2 phase [14], could

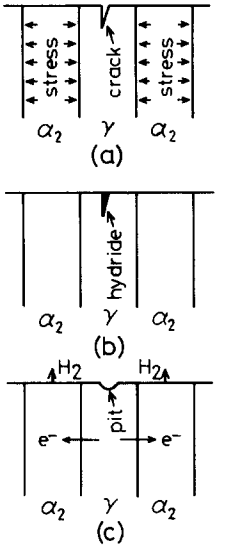

Fig. 10. Schematic representations of possible models for crack or pit formation during cathodic charging: (a) crack formation due to expansion of α_2 phase; (b) crack formation due to hydride formation in γ phase; (c) pit formation due to galvanic potential difference between α_2 and γ phases.

experience compressive stress due to the expansion of the α_2 phase, so that cracks could be produced within the γ phase. However, it is difficult for this model to explain the hydride formation in/on the γ phase. The second model (Fig. 10(b)) is due to hydride formation in the γ phase. This means that the γ phase in the two-phase coexisting grains takes up much more hydrogen than the α_2 phase or single γ grains, so that cracking could easily occur within the γ phase. It seems

for this model that there is a great difference from the gaseous hydrogen sorption. However, again we do not observe any damage within the equiaxed γ grains, so that complicated interactions during cathodic charging could occur only within the γ phase in the two-phase coexisting grains. The third model (Fig. 10(c)) is due to a galvanic potential difference between the α_2 and γ phases in acid solutions. In this model the α_2 phase acts as a noble metal while the γ phase acts as an active (less noble) metal, so that a galvanic potential difference between the α_2 and γ phases would be produced. The electrons in the γ phase move towards the α_2 phase and then titanium or aluminium ions dissolve in the acid solutions from the γ phase, so that pits could be produced within the γ phase. From the α_2 phase, gaseous hydrogen would be generated. This electrochemical model would be effective in acid solutions, and a two-phase or chemical compositional difference in alloys should be necessary to produce the galvanic potential difference, so that this reaction could be seen in two-phase alloys only by cathodic charging or in acid solutions but could not be seen by gaseous hydrogen charging. These three models are all possible, but it is difficult at this time to determine which model describes the phenomena best. An etching experiment in an acid solution is now under way to determine whether the third model is effective and the results will be reported elsewhere.

It is considered that the current density for hydrogen charging influences the hydrogen distribution and crack formation on sample surfaces. The current density applied in this study is somewhat higher compared with the charging condition shown in Table 1. Hydrogen charging with lower current density may also be needed for further study. Transmission electron microscopy observation of microstructures is now in progress and will be reported elsewhere.

5. Conclusions

(1) A (TiAl)H_x hydride with a tetragonal crystal structure and lattice parameters $a=0.452$ nm and $c=0.326$ nm ($c/a=0.721$) forms in Ti–42Al, Ti–45Al and Ti–50Al two-phase ($\alpha_2+\gamma$) alloys.

(2) Hydrogen charging induces crack formation after a short charging time, while additional charging produces pits within the γ phase and in two-phase ($\alpha_2+\gamma$) coexisting grains but no damage in the α_2 phase or equiaxed single γ grains.

(3) Weights of the samples decrease with increasing charging time as a result of the crack or pit formation. This is more drastic in the Ti–50Al alloy than in the Ti–42Al and Ti–45Al alloys.

(4) The hydride phase is thermally stable at temperatures up to about 550 K (277 °C) and dissociates at temperatures between 673 K (400 °C) and 723 K (450 °C).

Acknowledgments

The authors are grateful to Mr. A. Mitsuhashi, Mitsubishi Materials Corporation, for provision of the homogenized ingots and to Professor T.R. McNelley, US Naval Postgraduate School, for many helpful discussions.

References

[1] H.A. Lipsitt, *MRS Symp. Proc., 39* (1985) 351.
[2] N.S. Stoloff, Hydrogen effect on material behavior, in N.R. Moody and A.W. Thompson (eds.), *Proc. Fourth Int. Conf. on Effect of Hydrogen on the Behavior of Materials,* TMS, Warrendale, PA, 1990, p. 486.
[3] W.Y. Chu and A.W. Thompson, *Metall. Trans. A, 23* (1992) 1299–1312.
[4] A. Takasaki, K. Ojima and Y. Taneda, *Scr. Metall. Mater., 28* (1993) 1483–1487.
[5] M. Gao, J.B. Boodey, R.P. Wei and W. Wei, *Scr. Metall. Mater., 27* (1992) 1419–1424.
[6] E. Manor and D. Eliezer, *Scr. Metall., 23* (1989) 1313–1318.
[7] D. Eliezer, J. Haddad, M. Dangur and F.H. Froes, *Scr. Metall. Mater., 27* (1992) 845–850.
[8] P. Rozenak and M. Dangur, *J. Mater. Sci., 27* (1992) 2273–2278.
[9] W.Y. Chu, A.W. Thompson and J.C. Williams, *Acta Metall. Mater., 40* (1992) 455–462.
[10] Y. Zhang, Y. Wang, Y.B. Wang, W.Y. Chu and C.M. Hsiao, *Scr. Metall. Mater., 29* (1993) 975–980.
[11] J. Gao, Y.B. Wang, W.Y. Chu and C.M. Hsiao, *Scr. Metall. Mater., 27* (1992) 1219–1222.
[12] Y. Combres, S. Tsuyama and T. Kishi, *Scr. Metall. Mater., 27* (1992) 509–514.
[13] A.W. Thompson, Environmental effects on advanced materials, in R.H. Jones and R.E. Ricker (eds.), *Proc. Conf. on Environmental Effects on Advanced Materials,* TMS, Warrendale, PA, 1991, p. 21.
[14] F.H. Froes, C. Suryanarayana and D. Eliezer, *J. Mater. Sci., 27* (1992) 5113–5140.